Available online at www.sciencedirect.com

ScienceDirect

www.journals.elsevier.com/journal-of-environmental-sciences

JOURNAL OF ENVIRONMENTAL SCIENCES

www.jesc.ac.cn

Vertical distribution of aerosol optical properties based on aircraft measurements over the Loess Plateau in China

Junxia Li[1,2], Xingang Liu[3,], Liang Yuan[2], Yan Yin[2], Zhanqing Li[4], Peiren Li[1], Gang Ren[1], Lijun Jin[1], Runjun Li[4], Zipeng Dong[4,5], Yiyu Li[1], Junmei Yang[1]*

1. *Weather Modification Office of Shanxi Province, Taiyuan, Shanxi 030032, China. E-mail: ljx22258@126.com*
2. *Key Laboratory for Aerosol-Cloud-Precipitation of China Meteorological Administration, Nanjing University of Information Science and Technology, Nanjing, Jiangsu 210044, China*
3. *State Key Laboratory of Water Environment Simulation, School of Environment, Beijing Normal University, Beijing 100875, China*
4. *College of Global Change and Earth System Science, Beijing Normal University, Beijing 100875, China*
5. *Meteorological Institute of Shaanxi Province, Xi'an, Shaanxi 710017, China*

ARTICLE INFO

Article history:
Received 23 October 2014
Revised 19 January 2015
Accepted 26 January 2015
Available online 16 May 2015

Keywords:
Vertical distribution
Optical properties
Aircraft measurements
The Loess Plateau

ABSTRACT

Vertical distributions of aerosol optical properties based on aircraft measurements over the Loess Plateau were measured for the first time during a summertime aircraft campaign, 2013 in Shanxi, China. Data from four flights were analyzed. The vertical distributions of aerosol optical properties including aerosol scattering coefficients (σ_{sc}), absorption coefficients (σ_{ab}), Angström exponent (α), single scattering albedo (ω), backscattering ratio (β_{sc}), aerosol mass scattering proficiency (Q_{sc}) and aerosol surface scattering proficiency (Q'_{sc}) were obtained. The mean statistical values of σ_{sc} were 77.45 Mm^{-1} (at 450 nm), 50.72 Mm^{-1} (at 550 nm), and 32.02 Mm^{-1} (at 700 nm). The mean value of σ_{ab} was 7.62 Mm^{-1} (at 550 nm). The mean values of α, β_{sc} and ω were 1.93, 0.15, and 0.91, respectively. Aerosol concentration decreased with altitude. Most effective diameters (ED) of aerosols were less than 0.8 μm. The vertical profiles of σ_{sc}, α, β_{sc}, Q_{sc} and Q'_{sc} showed that the aerosol scattering properties at lower levels contributed the most to the total aerosol radiative forcing. Both α and β_{sc} had relatively large values, suggesting that most aerosols in the observational region were small particles. The mean values of σ_{sc}, α, β_{sc}, Q_{sc}, Q'_{sc}, σ_{ab} and ω at different height ranges showed that most of the parameters decreased with altitude. The forty-eight hour backward trajectories of air masses during the observation days indicated that the majority of aerosols in the lower level contributed the most to the total aerosol loading, and most of these particles originated from local or regional pollution emissions.

Introduction

Atmospheric aerosols directly affect the Earth's radiative budget by scattering and absorbing solar and thermal radiation (Haywood and Shine, 1997), and indirectly by acting as cloud condensation nuclei or ice nuclei in cloud formation, thus affecting the optical properties and lifetime of clouds, and furthermore, modifying the precipitation regime. Atmospheric aerosols also have adverse effects on environmental quality including atmospheric quality, visibility (Waggoner et al., 1981; Horvath, 1995), and human health. The spatial and temporal variations of radiative forcing by aerosols are strongly influenced

* *Corresponding author*. E-mail: lxgstar@126.com (Xingang Liu).

http://dx.doi.org/10.1016/j.jes.2015.01.021

by the variability of aerosol concentration distributions and optical properties on local to regional scales. The aerosol geographical and temporal distributions are very variable due to diverse emission sources, particle transformations and different removal processes. All these factors cause large uncertainties in evaluating the effects of aerosols on both climate and the environment. For this reason, many studies, including observational studies and numerical simulations, have been carried out to understand the physical, chemical, and optical properties of aerosols (*e.g.*, Kleefeld et al., 2002; Adam et al., 2004; Elias et al., 2006; Fischer et al., 2011; Li et al., 2007; Yan, 2007; Sun et al., 2014; Wang et al., 2014; Zhao et al., 2014) and their effects on climate radiative forcing, clouds, and precipitation (Yin et al., 2002, 2010).

Till now, most studies focusing on aerosol optical properties have been carried out from the ground, and some measurements were conducted focusing on variations of aerosol optical properties in China (Qiu and Takeuchi, 2001; Zhang et al., 2002, 2004; Xu et al., 2002, 2004; Yan et al., 2008; Liu et al., 2012; Tao et al., 2014). There is still an urgent need to better understand the vertical distributions of aerosol optical properties. Aircraft observations can afford the principal advantage of yielding detailed information on aerosol properties with height, albeit within short time periods over geographic areas of limited extent, thereby enabling the question of aerosol optical properties in the vertical direction to be addressed (Bodhaine et al., 1991; Hänel, 1998; Sheridan and Ogren, 1999; Welton et al., 2002; Anderson et al., 2003; Han et al, 2003; Raut and Chazette, 2008; Li et al., 2011, 2012).

However, because of the strict control of airspace and high operating costs, there is still a lack of aircraft observations of aerosol optical properties in the lower troposphere over urban and rural areas, especially in the central and eastern regions of northern China. It is therefore a major objective of this paper to evaluate the uncertainty of measured aerosol properties such as aerosol spatial distribution, particle size distribution, particle scattering and backscattering coefficients, particle absorption coefficients, particle single scattering albedo, and other properties through aircraft measurements to provide valuable observation data for regional model calculations on aerosol and climate.

Shanxi Province is located in the Loess Plateau of northern China, and the north China plain lies to the east of this region. As one of the most important heavy chemical bases of China, the mixture of heavy air pollution from industrial activities results in a rather complex nature for aerosol optical properties in the local region. However, till now, few studies have been reported on measurements of the important aerosol properties and especially the vertical distribution of these properties in Shanxi province. As a key part of the International Aerosol-CCN-Cloud Closure Experiment (ACCCExp-2013), an airborne campaign was conducted in August 2013 in Shanxi Province on the Loess Plateau of China. Comprehensive observations of atmospheric aerosol characteristics in this region were collected for the first time. In this paper, the characteristics and vertical variation of aerosol optical properties are analyzed involving the statistical properties of the optical characteristics of aerosols such as aerosol scattering coefficients (σ_{sc}), backscattering coefficients (σ_{bsc}), Angström exponent (α), backscattering ratio (β_{sc}), mass scattering efficiency (Q_{sc}), surface scattering efficiency (Q'_{sc}), absorption coefficients (σ_{ab}) and single scattering albedo (ω), as well as the vertical distributions of these parameters, vertical profiles of aerosol concentration and particle size, the correlation between aerosol concentration and σ_{sc}, and the backward trajectories of air masses.

1. Description of the field campaign

1.1. Observation area

Shanxi Province is located in northern China. The Loess Plateau covers most of the province, and the average surface altitude of the entire province is above 1000 m. Shanxi province connects with the north China plain in the east, and Hebei province and Beijing city are at the east of the province. Shanxi is situated in the temperate continental monsoon climate zone. It is an important energy and chemical industrial center of China. In conjunction with the rapid economic growth in the region, the increase in industrial emissions of anthropogenic aerosol particles has a strong impact on the regional air quality and climate. This has garnered much attention from the public in recent years. The field observation was carried out in the central region of Shanxi Province, and three main observatories were included in this study: Taiyuan (112.55°E, 37.867°N, altitude 778 m above sea level, or asl), Wenshui (112.14°E, 37.26°N, altitude 800 m asl), and Xinzhou (112.70°E, 38.73°N, altitude 800 m asl). Fig. 1 shows the map of Shanxi province and the locations of the three sites. The flight observation was mainly carried out around the three sites.

1.2. Instruments and measurements

A Y-12 turboprop airplane was used as an aerosol observation platform. The typical speed of the aircraft was about 60–70 m/sec and the rate of climb or descent of the aircraft

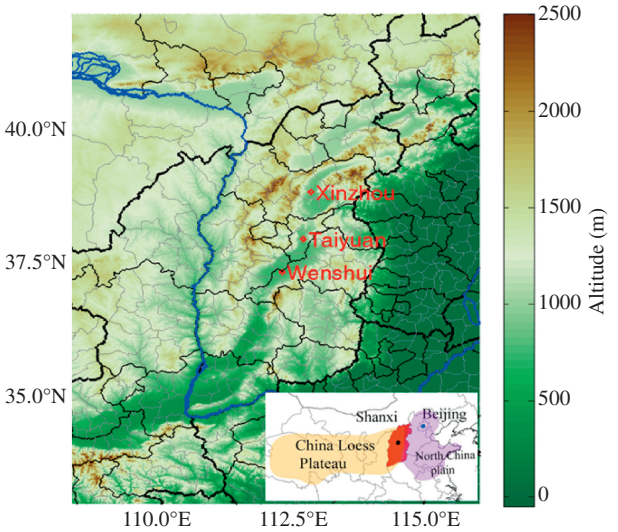

Fig. 1 – Map of Shanxi province over which flights were made and locations of the three main aerosol observatories (Taiyuan, Wenshui, and Xinzhou). The inert map shows the location of the observation area in China, in which the red shaded area represents Shanxi province.

was about 2–5 m/sec. It was equipped with multiple aerosol measurement instruments to determine aerosol properties, and each instrument was calibrated and tested rigorously during a ground-based campaign prior to the airborne campaign to ensure instrument performance. Two sample inlets are on the top of the airplane, and both were designed to minimize aerosol loses. The inlets connect to the measurement instruments with a direct sample path to avoid turns or corners as much as possible.

A three-wavelength (450, 550, 700 nm) integrating nephelometer (Model 3563, TSI, USA) was constructed for airborne measurements of the scattering (σ_{sc}) and backscattering coefficients (σ_{bsc}). Aerosol scattering coefficients could be characterized in the three-dimensional atmosphere with good resolution in both time and space. The nephelometer was calibrated by using CO_2 as high span gas and filtered zero air as low span gas. This instrument draws the ambient air through a temperature-controlled inlet at flow rate of 5 L/min. The averaging time was set to 10 sec. Scattering by aerosols is strongly dependent on relative humidity (RH) because of the hygroscopic growth nature of atmospheric aerosols (Horvath, 1996; Liu et al., 2008). The scattering coefficient shows a minimum variation below 50% RH and a slow increasing behavior up to about 60% RH (Anderson and Ogren, 1998; Xu et al., 2002; Liu et al., 2013). During the flight experiment period, a diffusion dryer was connected before the sample gas entered into the nephelometer. The RH measured within the nephelometer chamber was in the range 11.3%–46% with mean values of 25%, and the light-scattering measurements presented in this study can be considered as dry.

A multi-angle absorption photometer (MAAP5012, Thermo. Electron., USA) was used to record black carbon (BC) concentration and light absorption at a wavelength of 670 nm. The MAAP drew the ambient air at constant flow rate of 16.67 L/min. The total method uncertainty for the aerosol light absorption coefficient inferred from MAAP measurements was around 12% (Petzold and Schönlinner, 2004; Petzold et al., 2005).

A passive cavity aerosol spectrometer probe (PCASP-100X, DMT, USA) was equipped to observe aerosol particles with diameters ranging from 0.1–3.0 μm in 30 bins of variable size with a frequency of 1 Hz. The PCASP is calibrated by using polystyrene latex spheres (PSL) by Particle Metrics Inc. (PMI) every year before the measurements take place. Aerosol concentration and particle size were derived from PCASP data.

Meteorological parameters such as ambient temperature (*T*) and RH and real-time locations such as longitude, latitude, and altitude were also measured and recorded by an air-data probe device (AMMIS-20, DMT, USA) during the flights.

Data from four flights were collected for the study. The dates of the flights were 13, 19, 20, 28 August 2013. The plane was based at Taiyuan Wusu International Airport and flew from there to Wenshui or Xinzhou. Flight segments started at a specific height and proceeded in downward spirals. Measurements were taken during 5-min periods at 300-m altitude intervals. Flight details are given in Table 1, and the flight tracks are shown in Fig. 2.

All times are in China Standard Time (CST) and altitudes are heights above sea level in this study.

1.3. Methodologies and parameters

Aerosol scattering coefficients (σ_{sc}) and backscattering coefficients at three wavelengths (450, 550 and 700 nm) can be obtained directly from the nephelometer, and all the data observed were subjected to truncation correction and recalculated. The black carbon (BC) concentration ($[BC]_{conc.}$) was obtained from the MAAP, and the light absorption at the wavelength of 550 nm was calculated based on Eq. (1) (MAAP Specification).

$$\sigma_{ab} = 6.6 \times [BC]_{conc.} \times \frac{670}{550} \quad (1)$$

Data on aerosol concentration and size were from PCASP. All of the concentration data and effective diameter (ED) data from PCASP were recalculated and corrected because the data from the PCASP in the first bin are inaccurate due to the detection limit of the instrument, so they were eliminated from the analysis.

In addition to the σ_{sc} measurements, the Angström exponent (α), which characterizes the wavelength dependence of σ_{sc}, was obtained, thus providing information on the size distribution of the particles, that is, the relative amount of fine and coarse

Table 1 – Flight summary.

Date	Time range	Weather condition	Domain covered	Vertical height (m)	Instruments
2013-08-13	15:05–16:22 pm	Small amount of light cumulus, haze	Taiyuan, Wenshui (111.8–112.7°E, 37.3–38.0°N)	778–3800	Nephelometer, PCASP, AIMMS-20
2013-08-19	16:39–18:30 pm	Cloudless	Taiyuan, Wenshui (111.8–112.7°E, 37.3–38.0°N)	778–3800	Nephelometer, PCASP, AIMMS-20
2013-08-20	22:16–23:53 pm	Small amount of clouds, haze	Taiyuan, Wenshui (111.8–112.7°E, 37.0–38.0°N)	778–3800	Nephelometer MAAP, PCASP, AIMMS-20
2013-08-28	17:38–20:15 pm	Clear	Taiyuan, Xinzhou (112.2–112.9°E, 37.6–39.0°N)	778–4300	Nephelometer MAAP, PCASP, AIMMS-20

MAAP: multi-angle adsorption photometer; PCASP: passive cavity aerosol spectrometer probe; AIMMS: air-data probe device.

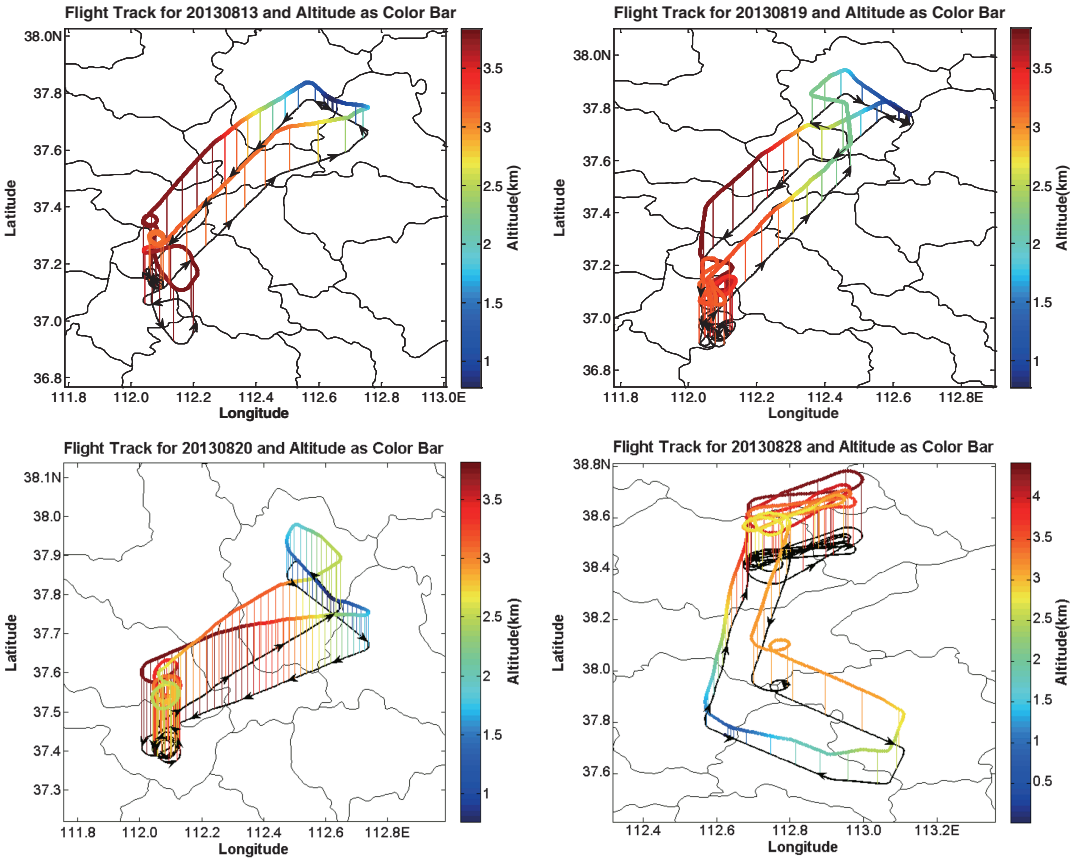

Fig. 2 – Four flights' tracks on 13, 19, 20, and 28 August, 2013.

particles, which differs according to the aerosol type (Seinfeld and Pandis, 1998). The Angström exponent was calculated according to Eq. (2).

$$\alpha = \frac{-\log\left[\sigma_{sc(700nm)}/\sigma_{sc(450nm)}\right]}{\log(700/450)} \quad (2)$$

The ratio of aerosol backscatter coefficients to total scattering coefficients (σ_{bsc}/σ_{sc}) is another very important parameter for the determination of fine particle content within the aerosol loading, which is called the backscattering ratio (β_{sc}). The ratio is given by Eq. (3).

$$\beta_{sc} = \frac{\sigma_{bsc}}{\sigma_{sc}} \quad (3)$$

The simultaneous measurements of aerosol mass concentration ($M_{aerosol}$) and scattering coefficients allowed the estimation of the mass scattering efficiency (Q_{sc}) and surface scattering efficiency (Q'_{sc}), defined as the ratio of the scattering coefficient to the mass concentration or surface concentration ($S_{aerosol}$), as shown by Eqs. (4) and (5). Both of the parameters can characterize the particles' light scattering capacity by unit mass or surface, and they are very important parameters for climate modeling studies (Zhang et al., 2004).

$$Q_{sc} = \sigma_{sc}/M_{aerosol} \quad (4)$$

$$Q'_{s\ c} = \sigma_s/_c S_{a\ e} \quad (5)$$

Based on the measurements of σ_{sc} and σ_{ab}, the single scattering albedo (SSA) at 550 nm ($\omega_{(550\ nm)}$) was calculated. The single scattering albedo is defined as the ratio of the aerosol scattering coefficient to the extinction coefficient (sum of the absorption and scattering coefficient), see Eq. (6).

$$\omega = \frac{\sigma_{sc}}{\sigma_{sc} + \sigma_{ab}} \quad (6)$$

This parameter is especially important in the estimation of direct aerosol radiative forcing. SSA can visually show the relationship between aerosol scattering and absorption function, and can be used for studying the radiation force at the top of atmosphere. The value of SSA is different for aerosols of different sizes and different chemical compositions. Most SSA values of aerosols in the northern hemisphere are in the range of 0.85–0.95 (Dubovik et al., 2002).

2. Results and discussion

2.1. Statistical characteristics of aerosol optical properties

Table 2 shows the statistical summary of the aerosol optical properties and aerosol concentration and size values in this experiment period. The mean (standard deviation) σ_{sc} at 450, 550, and 700 nm were 77.45 ± 96.76, 50.72 ± 61.5, and 32.02 ± 36.85 Mm^{-1}, and the mean σ_{bsc} at each wavelength were 9.18 ± 10.36, 7.04 ± 7.95, and 5.69 ± 6.96 Mm^{-1}, respectively.

Table 2 – Statistical summary of aerosol optical properties.

Parameter	Max.	Min.	Mean ± S.D.	Median
$\sigma_{sc\ (450\ nm)}$ (Mm^{-1})	511.7	0.96	77.45 ± 96.76	47.66
$\sigma_{sc\ (550\ nm)}$ (Mm^{-1})	326.7	0.44	50.72 ± 61.5	32.93
$\sigma_{sc\ (700\ nm)}$ (Mm^{-1})	195.5	0.15	32.02 ± 36.85	21.37
$\sigma_{bsc\ (450\ nm)}$ (Mm^{-1})	53.8	0.01	9.18 ± 10.36	6.16
$\sigma_{bsc\ (550\ nm)}$ (Mm^{-1})	40	0.1	7.04 ± 7.95	4.71
$\sigma_{bsc\ (700\ nm)}$ (Mm^{-1})	36.11	0.04	5.69 ± 6.96	3.41
$\sigma_{ab\ (550\ nm)}$ (Mm^{-1})	23.96	1.05	7.62 ± 7.55	4.98
$[BC]_{conc.}$ ($\mu g/m^3$)	2.98	0.13	0.95 ± 0.94	0.62
α	5.02	0.03	1.93 ± 0.46	1.91
$\beta_{sc\ (550nm)}$	0.75	0.02	0.15 ± 0.06	0.15
$\omega_{(550nm)}$	0.98	0.65	0.91 ± 0.05	0.93
Number conc. (cm^{-3})	7238.5	75.6	2162.7 ± 1785.3	1578
Volume conc. ($\mu m^3/cm^3$)	119.2	0.84	24.5 ± 21.8	16.2
Mass conc. ($\mu g/m^3$)	178.7	1.26	36.75 ± 32.68	24.25
Surface conc. ($\mu m^2/cm^3$)	1603.3	9.4	364.4 ± 331.6	214
ED (μm)	2.63	0.1	0.5 ± 0.5	0.32

σ_{sc}: aerosol scattering coefficients; σ_{bsc}: backscattering coefficients; σ_{ab}: absorption coefficients; $[BC]_{conc.}$: the black carbon (BC) concentration; α: Angström exponent; β_{sc}: backscattering ratio; ω: the single scattering albedo; ED: effective diameter.

The values of BC concentration ranged from 0.13 to 2.98 $\mu g/m^3$ with the mean value of 0.95 ± 0.94 $\mu g/m^3$, which corresponded to the calculated aerosol $\sigma_{ab\ (550\ nm)}$ in the range 1.05–23.96 Mm^{-1}, and with the mean value of 7.62 ± 7.55 Mm^{-1}. It should be noted that the large standard deviation for each variable reflected the strong fluctuation of the measured aerosol properties. The values of α ranged from 0.03 to 5.02 with the mean value of 1.93 ± 0.46. The average value of β_{sc} was 0.15 ± 0.06. According to the calculation based on Mie theory, the ratio will be larger than 0.10 if the particles' diameters are under about 1.5 μm. So, the relatively high values of both α and β_{sc} indicated that the scattering is dominated by fine particles, and a larger fraction of submicron particles dominated the total aerosol loading in the region during the experiment. The statistical results show that the mean and median values of $\omega_{(550\ nm)}$ obtained were 0.91 ± 0.05 and 0.93. The mean values are: aerosol number concentration 2162.7 ± 1785.3 cm^{-3}; volume concentration 24.5 ± 21.8 $\mu m^3/cm^3$; mass concentration 36.75 ± 32.68 $\mu g/m^3$; surface concentration 364.4 ± 331.6 $\mu m^2/cm^3$. The ED of most aerosol particles was smaller than 0.8 μm during the observation, and the mean value was 0.5 μm.

The measure obtained data were compared with results recorded in other sites in China (see Table 3). For instance, the aerosol scattering coefficient values obtained in Beijing are much larger than the Yulin, Lanzhou, and SDZ sites, and those values were comparable to those obtained at a rural area of the Yangtze Delta Region in eastern China and Chengdu in southwestern China. The aerosol scattering coefficient observed in this study is smaller than most of the other sites list in Table 3 except for Yulin and SDZ. The aerosol absorption coefficient obtained here is larger than that recorded in Yulin, comparable to SDZ, and smaller than other sites. The β_{sc} obtained here is nearly the same as that in Lanzhou, which indicates that most aerosol particles were small in the observation area. All of the ω in the table are in the range from 0.8 to 0.95, which is consistent with the results

Table 3 – Aerosol optical properties at other sites in China.

Site	Period	σ_{sc} (Mm^{-1})	σ_{ab} (Mm^{-1})	β_{sc}	ω	Instruments	Reference
PKU, Beijing (urban)	1999.06	488 (at 530 nm)	83 (at 565 nm)	n/a	0.81 (at 550 nm)	PSAP, Nephelometer M903	Bergin et al. (2001)
Yangtze delta region (rural)	1999.11	353 (at 530 nm)	23 (at 565 nm)	n/a	0.93	PSAP, Nephelometer M903	Xu et al. (2002)
Yulin (desert)	2001.04	158 (at 530 nm)	6 (at 565 nm)	n/a	0.95	PSAP, Nephelometer M903	Xu et al. (2004)
Lanzhou (urban)	2001–2002, winter	307 (at 450 nm) 226 (at 550 nm) 131 (at 700 nm)	n/a	0.16		Nephelometer M3563	Zhang et al. (2004)
SDZ (rural)	2003–2005	174.6 (at 525 nm)	17.5 (at 525 nm)	n/a	0.88 (at 525 nm)	Aethalometer AE31, Nephelometer M9003	Yan et al. (2008)
Bejing (rural)	2005.03	468 (at 550 nm)	65 (at 550 nm)		0.81–0.85	PSAP, Nephelometer M9003	Li et al. (2007)
Guangzhou (urban)	2004.10–11	463 (at 530 nm)	92 (at 530 nm)		0.84	PSAP, M903	Andreae et al. (2008)
PKU, Beijing (urban)	2005–2006	288 (at 525 nm)	56 (at 532 nm)		0.8 (525 nm)	Aethalometer AE16, Nephelometer M9003	He et al. (2009)
Shouxian, Anhui (rural)	2008.5–12	401 (at 550 nm)	29 (at 550 nm)		0.92	Nephelometer TSI 3563, PSAP	Fan et al. (2010)
Shanghai	2010.12–2011.3	293 (at 532 nm)	66 (at 532 nm)		0.81	Nephelometer M9003; Aethalometer, Model AE-31	Xu et al. (2012)
Xi'an	2009	525 (at 520 nm)	83			Nephelometer, Model Aurora1000	Cao et al. (2012)
Chengdu	2011	456 (at 520 nm)	96 (at 532 nm)		0.82	Nephelometer, Model Aurora1000G; Aethalometer, Model AE-31	Tao et al. (2014)
Taiyuan (urban)	2013.8 Near surface Total	189 (at 550 nm) 51	15 (at 550 nm) 7.6	0.15 0.15	0.94 0.91	Nephelometer TSI3563, MAAP M5012	This work

n/a: Not available.

of Dubovik et al. (2002). It must be pointed out that all the other measurements were taken from the ground, and are long-time-series observations. By contrast, the results in this study are from just four airborne measurements, and the data in Table 3 are the mean values observed below 1000 m height (The altitude of the ground surface is 778 m) during the flights, which cannot reflect the long-range state of the aerosol properties on the ground.

2.2. Vertical profiles of aerosol concentration and ED

Previous aircraft observational studies showed that aerosol vertical profiles have a close relationship with the PBL structure, including the vertical distribution of *T* and RH (*e.g.*, Johnson et al., 2000; Zhang et al., 2006). The vertical profile of aerosol is relatively uniform within the boundary layer, and decreases obviously with height above the boundary layer. Fig. 3 shows mean the vertical profiles of *T* and RH during each flight.

In all the flights, temperature decreased with height. A shallow temperature inversion layer (TIL) was seen at the height of 1500–2000 m on 13, 19 and 20 August, and another obvious TIL was observed between 3000 to 3500 m for the four flights. On 28 August, there was a deep TIL above 3800 m. The RH was relatively low on 19 August and the maximum value was no more than 60% in the vertical direction. The RH was higher at the height of 2000–2500 m on 20 August, and the maximum value was nearly 90%. In total, the RH values near the surface were low, and increased with height, and were

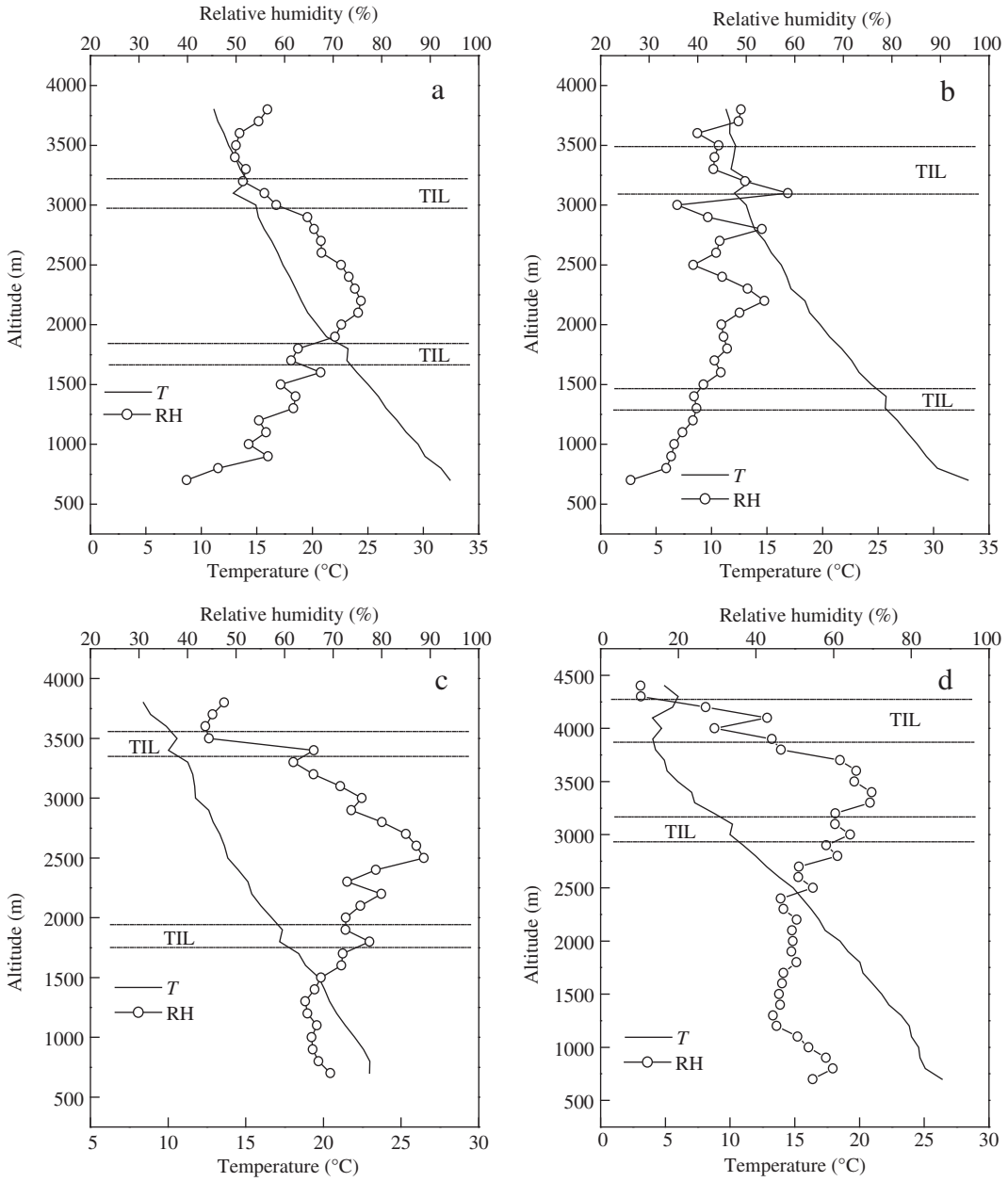

Fig. 3 – Vertical profiles of temperature (*T*) and relative humidity (RH) measured on 13 (a), 19 (b), 20 (c), and 28 August (d), 2013. TIL: temperature inversion layer.

relatively higher at the height range from 2000 to 3500 m, which may be because of the effects of light cumulus clouds occurring in these layers.

In terms of radiative forcing of climate, the sub-micrometer size range is most relevant for light scattering because it comprises particles with diameters comparable to the wavelength of the visible solar radiation (Cheng et al., 2008). Therefore, the concentration and size of aerosol particles from 0.1 to 3 μm are discussed first. Fig. 4 shows the mean vertical profiles of aerosol number concentration (Fig. 4a), mass concentration (Fig. 4b), surface concentration (Fig. 4c), and ED (Fig. 4d) of the four flights. 13 and 20 August were haze days, and the aerosol number concentration was high during these two days. Another two flights on 19 and 28 August were carried out on clear days. The vertical profiles of aerosol concentration showed different shapes in each flight because of different observation time ranges and different weather conditions. Looking at the profiles of mean value (black line with hollow circles), all of the aerosol concentrations stayed nearly uniform from the surface to 1500 m, then decreased sharply with height, which was similar to the results of Li et al. (2015). The first peak in aerosol concentration appeared around 1800 m, which was an obvious aerosol accumulation layer, and the second peak in aerosol concentration was seen at the height of 2300–2500 m. Combined with the vertical temperature profiles (Fig. 3), on most of the four flights two TILs occurring below 2000 m and above 3000 m were responsible for the two peaks of aerosol concentration in the vertical direction. On 28 August, the aerosol number concentration decreased from the surface with altitude initially, but then increased with altitude from 3300 m upward, which may be due to the deep TIL layer at the higher level of 3700 m on that day. Thus, weather conditions, especially the vertical profile of temperature, have a strong effect on the aerosol vertical distribution (Li et al., 2015).

In general, ED showed no obvious trend with altitude. Two peaks of ED were measured along the vertical direction. The first peak value of ED occurred between 2000–2500 m and another one appeared above 3500 m. Most ED of aerosols were less than 0.8 μm. Snider et al. (2000) showed that RH has an effect on aerosol particle size distributions. High RH values were seen

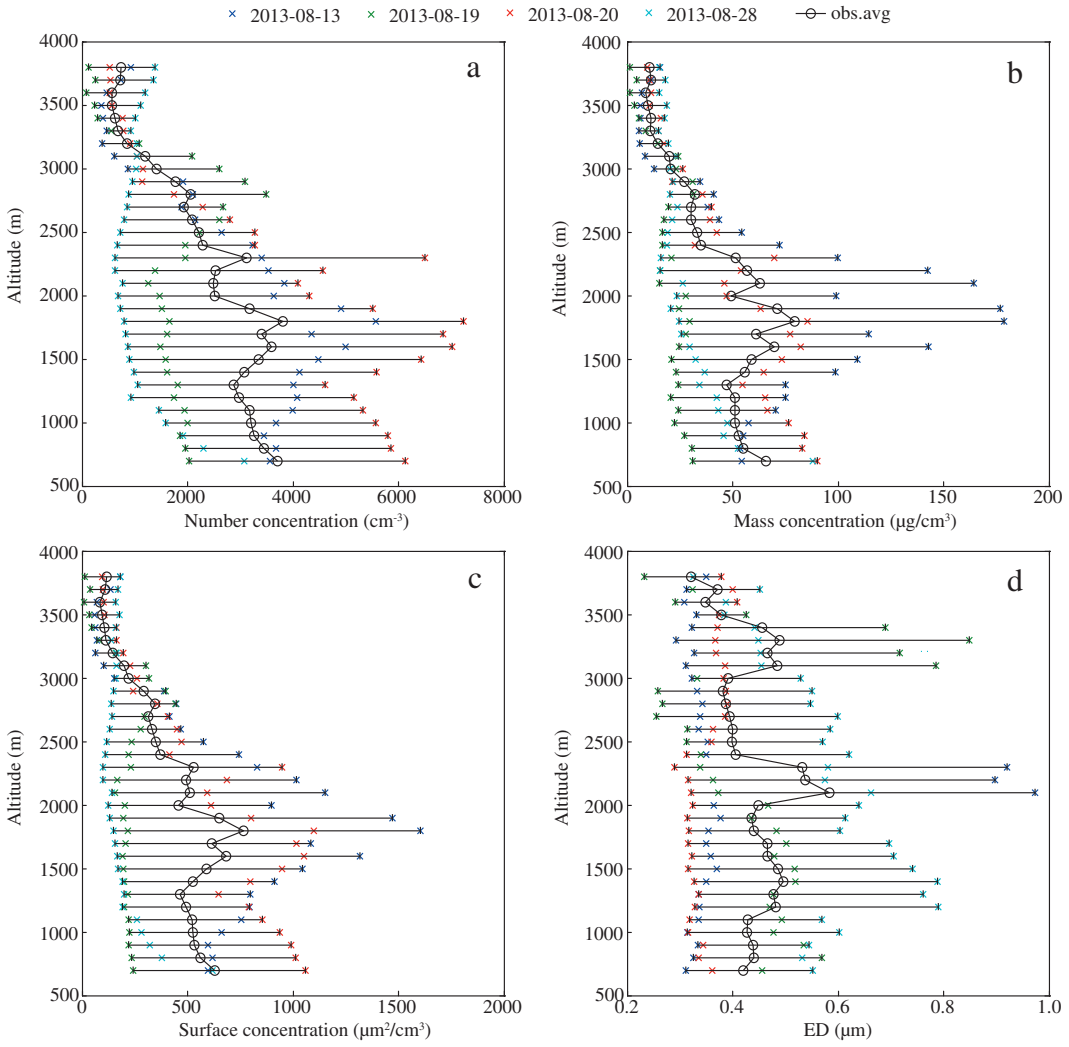

Fig. 4 – Vertical profiles of mean aerosol number concentration (a), mass concentration (b), surface concentration (c), and effective diameter (ED) (d) from all flights. Horizontal black lines: the range of values (minimum and maximum values) observed at each altitude level.

above 2000 m, and most of the peak values of ED were measured above 2000 m in this study, but no strict correlation between RH and aerosol size was seen. The ED represents the mean size of aerosols, so aerosols with different ED generally come from different sources. The combination of information from vertical profiles of aerosol concentration and ED can help us to determine the source of the aerosols. In this study, the majority of aerosols under 2000 m were fine mode particles with ED less than 0.5 μm, which suggests that these particles might originate from local or regional pollution emissions. Relatively large particles distributed at higher altitudes may suggest that these particles were transported to the region from desert areas afar.

Atmospheric aerosols are comprised of different chemical components and a variety of different-sized particles. The distribution of aerosol particle number density with particle size, known as the particle average spectrum distribution, is an important physical quantity used to describe the aerosol number size distribution. Aerosol particles in different areas and in different atmospheric environments have different spectrum distributions. A change in atmospheric conditions will change the particles' properties, leading to a change in particle spectrum. Fig. 5 shows the time series of aerosol spectrum distribution during the flight on 13 (Fig. 5a) and 20 August (Fig. 5b). On average, the magnitude of aerosol particle number concentration was about 10^3 cm^{-3}, and the maximum value of aerosol particle number concentration was more than 10^4 cm^{-3}. The peak in the aerosol number concentration was seen at 0.2–0.3 μm, and all of the large values appeared at the beginning or the end time of the flight when the airplane was near the ground at lower altitude. The aerosol number concentrations with ED larger than 0.5 μm were on the order of 10^2 cm^{-3}, and the aerosol number concentrations with ED larger than 0.8 μm were on the order of 10 cm^{-3} or less. So, fine particles with ED smaller than 0.5 μm comprised most of the total aerosol concentration during the flight experiment.

2.3. Vertical distributions of aerosol optical properties

2.3.1. Vertical profiles of aerosol scattering properties

Light scattering by atmospheric aerosol particles affects the Earth's energy balance and contributes to the negative radiative forcing of climate. Fig. 6 shows the vertical profiles of aerosol scattering coefficients ($\sigma_{sc\ (450\ nm)}$, $\sigma_{sc\ (550\ nm)}$, and $\sigma_{sc\ (700\ nm)}$) (Fig. 6a, b, c, d), Angstrom exponent (α), backscattering coefficient (β_{scat}) (Fig. 6a1, b1, c1, d1), aerosol mass scattering proficiency (Q_{sc}), and aerosol surface scattering proficiency (Q'_{sc}) (Fig. 6a2, b2, c2, d2) of the four flight measurements, respectively.

Generally, the values of σ_{sc} at 450, 550, and 700 nm decreased with altitude obviously for most flights, except on 19 August. On 13 and 20 August, two haze days, the values of σ_{sc} were relatively higher near the ground, and decreased with height gradually. On 13 August (Fig. 6a), the peak of σ_{sc} appeared at the height of 1500 m with the maximum values of 289.4, 200.9, and 131.6 Mm^{-1} at 450, 550, and 700 nm respectively. There were small amounts of light cumulus at the height range of 2000–2300 m, and σ_{sc} was reduced slightly at this level. On 20 August, there were more pollutants in the atmosphere, and the concentration of aerosols was higher. In Fig. 6c, the maximum value of σ_{sc} (511.7, 326.5, and 195.5 Mm^{-1} at 450, 550, and 700 nm, respectively) appeared near the ground, and there were two

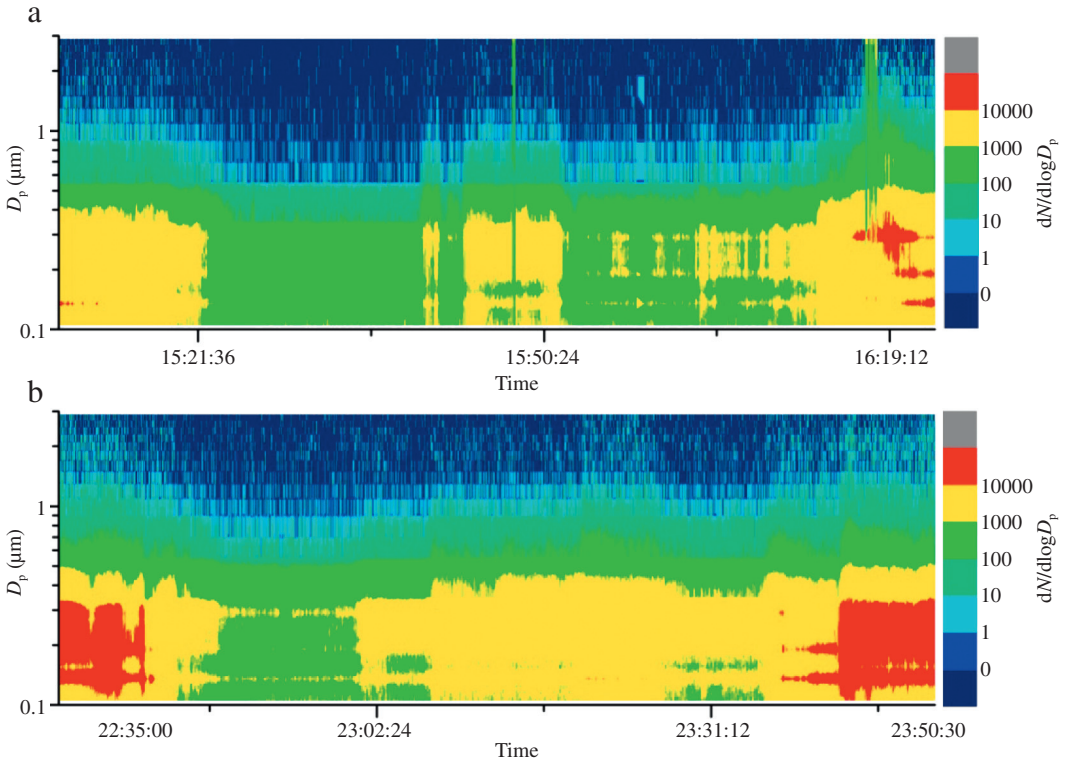

Fig. 5 – Time series of aerosol spectrum distribution during the flight on 13 (a) and 20 August (b). D_p: the aerosol particle size (diameter); dN/dlogD_p: the number concentration of aerosol particles in each size bin.

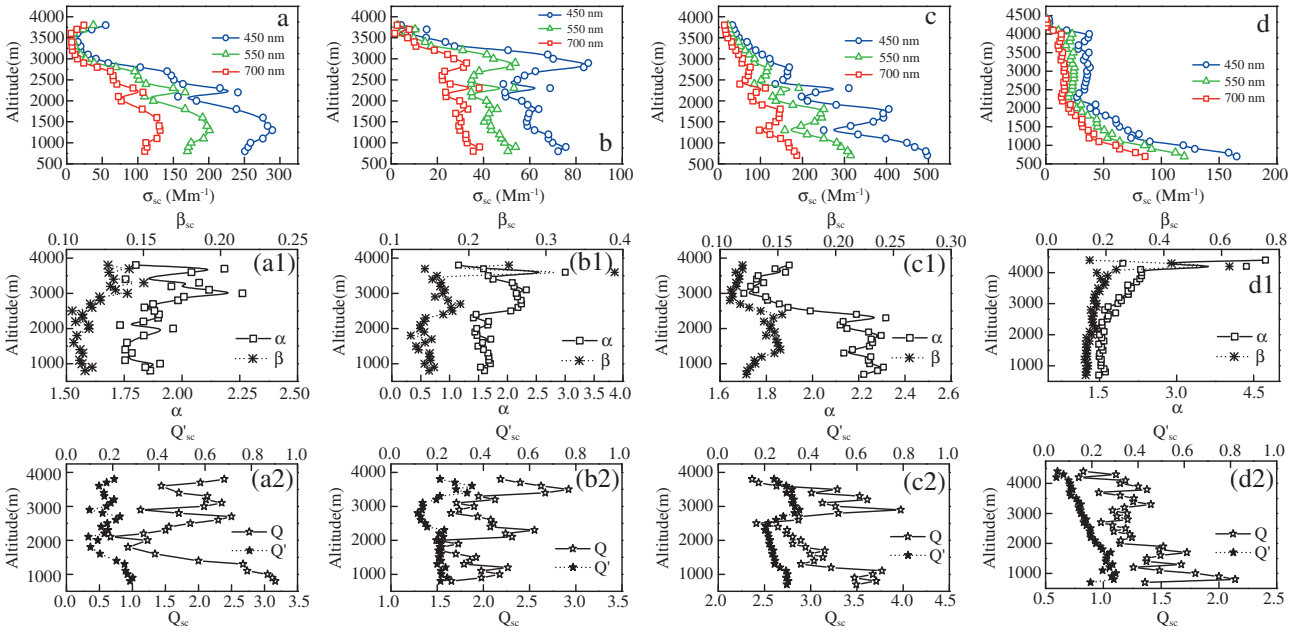

Fig. 6 – Vertical profiles of aerosol scattering coefficients (σ_{sc}) at 450, 550, and 700 nm, Angström exponent (α), backscattering ratio (β_{sc}), mass scattering efficiency (Q_{sc}) and surface scattering efficiency (Q'_{sc}) on 13 (a, a1, a2), 19 (b, b1, b2), 20 (c, c1, c2), and 28 August (d, d1, d2), 2013.

peaks of σ_{sc} at the heights of 1800 m and 2300 m. The flight was carried out at night on 20 August, and there were small amounts of clouds at the heights of 1000–1200, 1800–2300 and 3500–3700 m according to the flight records. So, the aerosol concentrations were lower because of the consumption effect within the cloud layers, which led to the decrease of σ_{sc} in these layers. Thus, both of the vertical profiles showed waves in the vertical direction on 13 and 20 August. August 19 was a clear day, and the value of σ_{sc} was smaller compared to the other three days. The σ_{sc} value changed slightly from the ground to 2700 m, and showed the peak value (120.5, 72.3, and 45.9 Mm^{-1} at 450, 550, and 700 nm) at the height of 3000 m. On 28 August, the maximum value of σ_{sc} (171.3, 117.3, and 83 Mm^{-1} at 450, 550, and 700 nm, respectively) appeared near the ground, and decreased smoothly with height. In total, the aerosol scattering properties in the lower layer (below 2000 m) contributed the most to the total aerosol radiative forcing, and this is consistent with the results of aircraft measurements by Sheridan and Ogren (1999).

The Angström exponent (α) is an intensive parameter that depends on the aerosol size distribution and increases with decreasing particle size. Aerosol type can be estimated through the Angström exponent. In situations where the scattering is dominated by coarse particles, α values tend to be lower than 1 or even close to 0. This is a typical signature of desert dust particles. On the other hand, when $\alpha > 1$, the scattering is dominated by smaller particles (Seinfeld and Pandis, 1998). The backscattering ratio (β_{sc}) is commonly required in radiative transfer models for the estimation of aerosol-scattered radiation reaching the ground (Iqbal, 1983). It is one of the parameters required for the measurement of Lidar, which can directly affect the accuracy of Lidar detection (Guasta and Marini, 2000). The higher the value of the ratio, the greater the content of fine particles. Fig. 6a1, b1, c1, d1 shows the vertical profiles of α and β_{sc} on 13 (Fig. 6a1), 19 (Fig. 6b1), 20 (Fig. 6c1), and 28 August (Fig. 6d1), 2013. In these figures, the vertical profiles of α and β_{sc} had the same change trend with altitude, and most of them changed within a small range. All the values of α were larger than 1 and the average value was about 1.9. Most of the β_{sc} increased a little gradually with altitude, with an average value of 0.15. Both of α and β_{sc} show relatively large values, suggesting that most aerosols in the observational space were small particles and the scattering was dominated by small particles.

Fig. 6a2, b2, c2, d2 shows the vertical profiles of Q_{sc} and Q'_{sc} on 13 (Fig. 6a2), 19 (Fig. 6b2), 20 (Fig. 6c2), and 28 August (Fig. 6d2), 2013. The Q_{sc} generally decreased from the surface to the height of 2000 m and then increased upward. The value ranged from 0.67 to 3.97 with the mean value of 2.06. The vertical profile of Q'_{sc} had the same trend as Q_{sc}, and the value changed in a small range from 0.05 to 0.35 with the mean value of 0.21.

In order to clearly portray the aerosol scattering properties at different altitudes, the mean values of σ_{sc}, α, β_{sc}, Q_{sc} and Q'_{sc} at different height range (every 1000 m average) are shown in Table 4. Most of the parameters decreased from near the surface to higher altitudes, except for β_{sc}. Parameters that characterize the vertical distribution of the aerosol scattering properties may be used as an important reference for parameterized schemes of local climate or radiation numerical models.

2.3.2. Aerosol concentration as a function of σ_{sc}

Aerosol number concentration, surface concentration, and mass concentration as a function of aerosol scattering coefficient are shown in Fig. 7. Data are from all flights. Linear fits were made to the data to determine the correlations between aerosol concentration and σ_{sc} without considering the influence of the chemical composition of aerosols. The correlation coefficients of the linear regressions are 0.93 (Fig. 7a), 0.91 (Fig. 7b) and 0.81 (Fig. 7c). This

Table 4 – Statistical values of aerosol scattering properties at different altitudes.

Altitude (m)	σ_{sc} (Mm^{-1})	σ_{bsc} (Mm^{-1})	α	β_{sc}	Q_{sc}	Q'_{sc}
778–1000	188.8 ± 110	23.7 ± 13	1.86 ± 0.35	0.13 ± 0.01	2.61 ± 0.87	0.27 ± 0.04
1000–2000	108.6 ± 84.8	14.9 ± 11.8	1.78 ± 0.31	0.14 ± 0.01	2.17 ± 0.76	0.24 ± 0.04
2000–3000	51.1 ± 37.8	7.1 ± 4.8	1.78 ± 0.26	0.15 ± 0.02	1.91 ± 0.77	0.19 ± 0.05
3000–4000	26.5 ± 19.1	3.9 ± 2.8	2.03 ± 0.53	0.16 ± 0.07	1.98 ± 0.79	0.19 ± 0.09

Data are presented as mean ± standard deviation.
Q_{sc}: mass scattering efficiency; Q'_{sc}: surface scattering efficiency.

suggested that a linear fit of aerosol number concentration with σ_{sc} was more suitable in this study.

2.3.3. Vertical distribution of aerosol absorption properties

Table 5 shows the statistical values of aerosol absorption properties at different altitudes during the flights on 20 and 28 August. The data are the mean values for 1000 m segments in the vertical direction. All the values of BC concentration, σ_{ab} and ω decreased from near the surface to higher altitudes. On 20 August, a haze day, the values of BC concentration and σ_{ab} were larger than those on 28 August, which may be due to the different observation areas, weather conditions and aerosol sources. The value of ω ranged from 0.9 to 0.95 with no obvious difference between the two flights.

2.4. Forty-eight hour backward trajectories of air masses

In order to analyze the source of aerosol particles over the observation region, the forty-eight hour backward trajectories of air masses were simulated during the experiment period by using the Hybrid of Single Particle Lagrangian Integrated Trajectory (Hysplit) model (Draxler and Hess, 1997) from the Atmosphere Research Laboratory (ARL) of the National Oceanic and Atmospheric Administration (NOAA) and the Australian Bureau of Meteorology. The American meteorological center global environmental prediction data assimilation system (NECP, GDAS) 1° × 1° meteorological field was adopted for modeling, and the backward trajectory end-station was Taiyuan station. Four heights above ground level (AGL) (500, 1500, 2500, 3500 m) were selected for the simulation. Fig. 8 shows the results of forty-eight hour backward trajectories of air masses on 13, 19, 20, and 28 August, 2013 in Taiyuan.

On 13 (Fig. 8a) and 20 August (Fig. 8c), the atmosphere was relatively stable and the vertical transport of aerosols was weak. The majority of aerosols below 2000 m height originated from local or regional pollutant emissions in the direction of the south and southeast region from Taiyuan. Particles distributed at higher altitudes were transported from the west areas afar. On 20 August (Fig. 8c), parts of the aerosols came from the high level (above 3000 m) transport because of the Gravity sedimentation effect, besides the local emissions. On 19 (Fig. 8b) and 28 August (Fig. 8d), there were very few aerosols from local ground emission and most of the aerosols were transported from the north and west areas afar and fell to lower level, because of gravity sedimentation from high levels above 3000 m. The combination of vertical distributions of aerosol concentration and aerosol optical properties suggested that the majority of aerosols in the lower level below 2000 m contributed most of the aerosol loading on 13 and 20 August, which led to high values of aerosol concentration and optical properties, and most of these particles originated from local or regional pollution emissions. Aerosols transported from the north

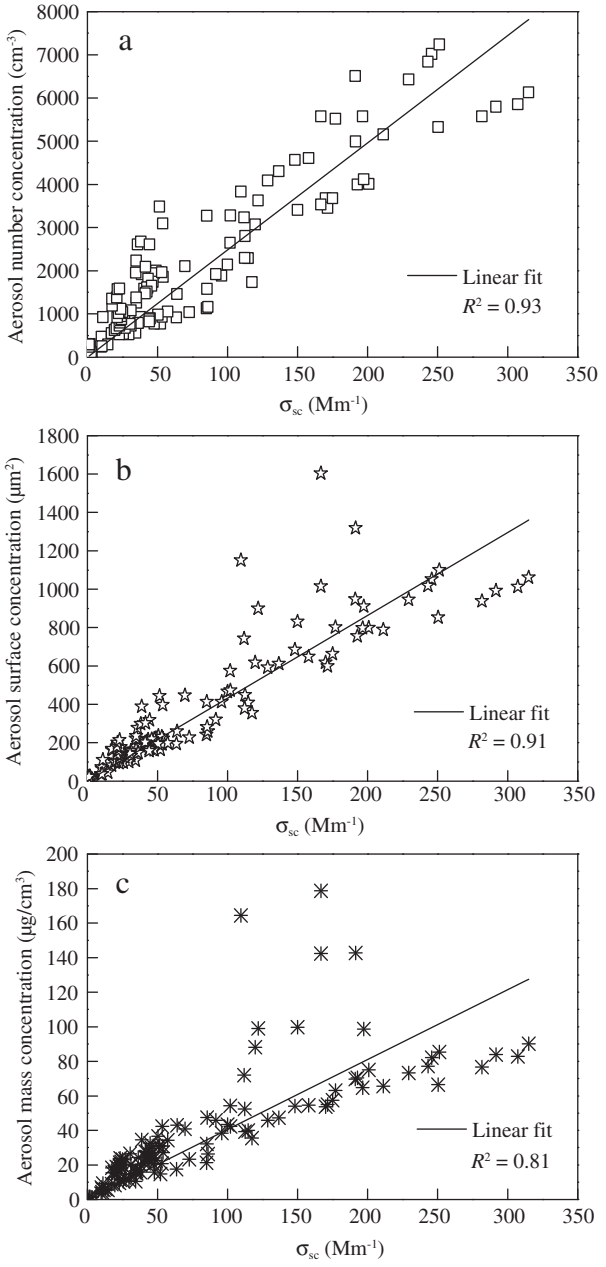

Fig. 7 – Aerosol number concentration (a), surface concentration (b), and mass concentration (c) as a function of σ_{sc}.

Table 5 – Statistical values of aerosol absorption properties at different altitudes.

Date	Altitude (m)	$[BC]_{conc.}$ ($\mu g/m^3$)	$\sigma_{ab\ (500\ nm)}$ (Mm^{-1})	ω
2013-8-20	778–1000	2.81 ± 0.15	22.58 ± 1.22	0.93 ± 0.00
	1000–2000	1.89 ± 0.91	15.16 ± 7.33	0.94 ± 0.02
	2000–3000	1.07 ± 0.8	8.63 ± 6.45	0.92 ± 0.05
	3000–4000	0.67 ± 0.61	5.32 ± 4.89	0.90 ± 0.11
2013-8-28	778–1000	0.86	6.91	0.95
	1000–2000	0.34	2.73	0.94
	2000–3000	0.25 ± 0.08	1.98 ± 0.65	0.92 ± 0.03
	3000–4000	0.26 ± 0.04	2.11 ± 0.33	0.89 ± 0.02

Data are presented as mean ± standard deviation.

and west areas dominated the observation regions on 19 and 28 August, which led to relatively lower values of aerosol concentration and optical properties.

3. Conclusions

The vertical profiles of aerosol concentration and size distributions as well as the aerosol optical properties were obtained through analyses of aerosol measurements collected during a summertime aircraft campaign over the Loess Plateau in China.

Statistical values of the aerosol properties in this experiment period were obtained and compared with results recorded in other sites in China. Both σ and β_{sc} showed relatively high values, indicating that the scattering was dominated by fine particles and a larger fraction of submicron particle loading in this region during the experiment.

Mean vertical profiles of aerosol concentration and ED were analyzed. The aerosol spectrum distribution showed that the average aerosol number concentrations were about 10^3 cm^{-3}. The peak in the aerosol number concentration was at 0.2–0.3 μm, and all of the large values appeared at lower altitude. Fine

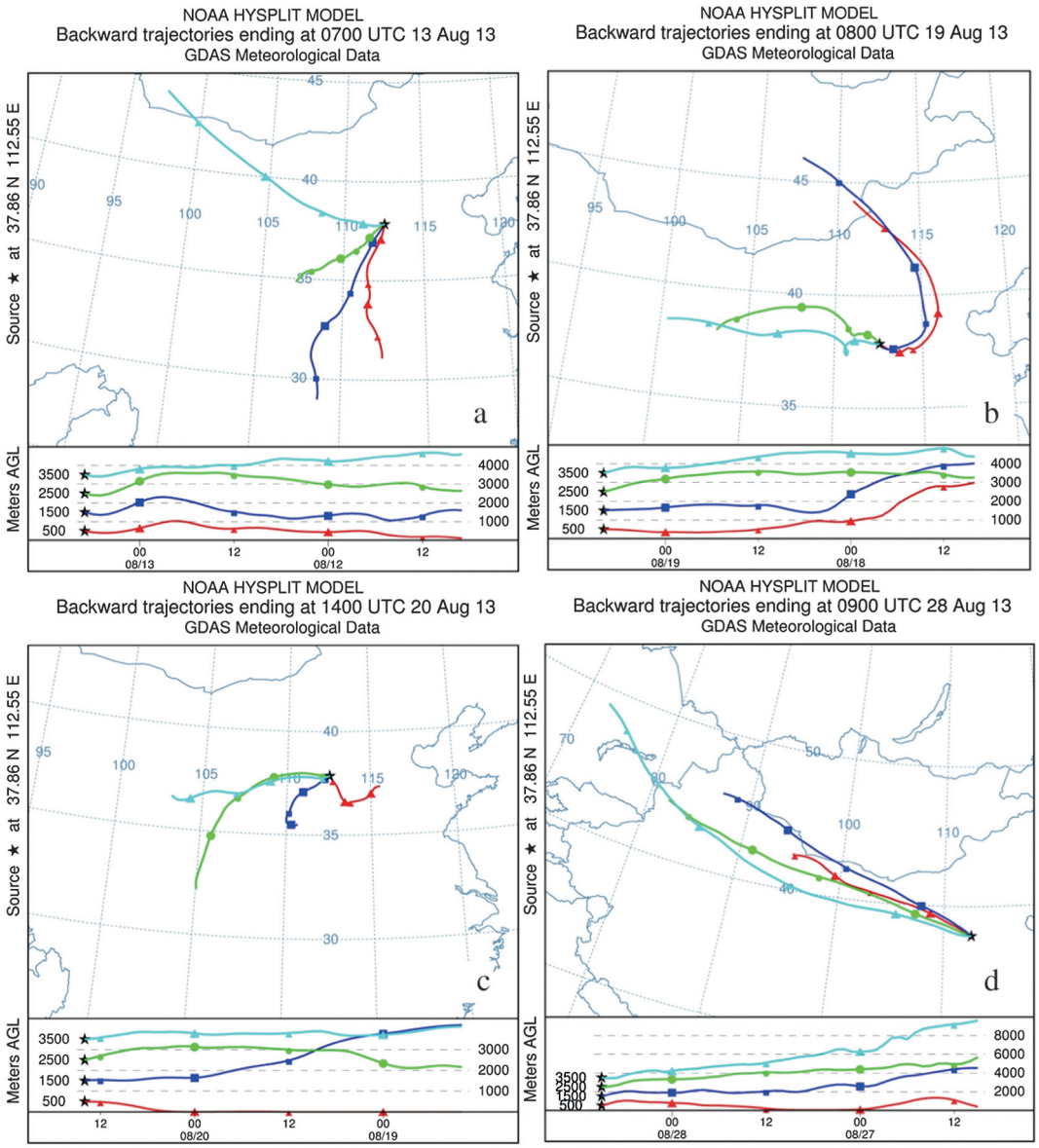

Fig. 8 – Forty-eight hour backward trajectories of air masses on 13 (a), 19 (b), 20 (c), and 28 August (d), 2013 in Taiyuan.

particles with ED smaller than 0.5 μm comprised most of the total aerosol concentration during the flight experiment.

The vertical profiles of σ_{sc}, α, β_{scat}, Q_{sc} and Q'_{sc} were studied. The aerosol scattering properties below 2000 m contributed the most to the total aerosol radiative forcing. The mean values of σ_{sc}, α, β_{sc}, Q_{sc} and Q'_{sc} at different height ranges showed that most of the parameters decreased with altitude. The values of BC concentration, σ_{ab} and ω decreased from the surface to higher altitude. Parameters that characterize the vertical distribution of aerosol optical properties can provide valuable references for parameterized schemes of local climate or radiation numerical models.

The forty-eight hour backward trajectories of air masses during the experiment period showed that the majority of aerosols in the lower level dominated the total aerosol loading, leading to high values of aerosol concentration and radiative forcing, and most of these particles originated from local or regional pollution emissions.

Acknowledgments

The study is supported partially by the Ministry of Science and Technology of China under its national key project on global change studies (No. 2013CB955804), the Special Fund for doctorate programs in Chinese Universities (No. 20113228110002), the Public Meteorology Special Foundation of MOST (No. GYHY201306065), and the Shanxi Meteorological Bureau Key Research Projects (No. SXKZDTC20140605).

REFERENCES

Adam, M., Pahlow, M., Kovalev, V.A., Ondov, J.M., Parlange, M.B., Nair, N., 2004. Aerosol optical characterization by nephelometer and lidar: the Baltimore Supersite experiment during the Canadian forest fire smoke intrusion. J. Geophys. Res. 109 (D16), D16S02. http://dx.doi.org/10.1029/2003JD004047.

Anderson, T.L., Ogren, J.A., 1998. Determining aerosol radiative properties using the TSI 3563 integrating nephelometer. Aerosol Sci. Technol. 29 (1), 57–69.

Anderson, T.L., Masonis, S.J., Covert, D.S., Ahlquist, N.C., Howell, S.G., Clarke, A.D., et al., 2003. Variability of aerosol optical properties derived from in situ aircraft measurements during ACE-Asia. J. Geophys. Res. 108 (D23). http://dx.doi.org/10.1029/2002JD003247 (CiteID8647).

Andreae, M.O., Schmid, O., Yang, H., Chanda, D., Yu, J., Zeng, L., et al., 2008. Optical properties and chemical composition of the atmospheric aerosol in urban Guangzhou, China. Atmos. Environ. 42 (25), 6335–6350. http://dx.doi.org/10.1016/j.atmosenv.2008.01.030.

Bergin, M.H., Cass, G.R., Xu, J., Fang, F., Zeng, L., Yu, T., et al., 2001. Aerosol radiative, physical, and chemical properties in Beijing during June 1999. J. Geophys. Res. 106 (D16), 17969–17980.

Bodhaine, B.A., Ahlquist, N.C., Schnell, R.C., 1991. Three-wavelength nephelometer suitable for aircraft measurement of background aerosol scattering coefficient. Atmos. Environ. 25 (10), 2267–2276.

Cao, J., Wang, Q., Chow, J.C., Watson, J.G., Tie, X., Shen, Z., et al., 2012. Impacts of aerosol compositions on visibility impairment in Xi'an, China. Atmos. Environ. 59, 559–566.

Cheng, Y.F., Zhang, Y.H., Hu, M., 2008. An Observation-based Method for Investigating the Atmospheric Aerosol Radiative Properties in Pearl River Delta of China. Science Press, Beijing.

Draxler, R.R., Hess, G.D., 1997. Description of the HYSPLIT_4 modeling system. NOAA Tech. Memo (ERL ARL-224).

Dubovik, O., Holben, B.N., Eck, T.F., Smirnov, E., Yoram, J., King, M.D., et al., 2002. Variability of absorption and optical properties of key aerosol types observed in worldwide locations. J. Atmos. Sci. 59 (3), 590–608.

Elias, T., Silva, A.M., Belo, N., Pereira, S., Formenti, P., Helas, G., et al., 2006. Aerosol extinction in a remote continental region of the Iberian Penı'nsula during summer. J. Geophys. Res. 111 (D14), D14204. http://dx.doi.org/10.1029/2005JD006610.

Fan, X., Chen, H., Xia, X., Li, Z., Cribb, M., 2010. Aerosol optical properties from the atmospheric radiation measurement mobile facility at Shouxian, China. J. Geophys. Res. 115 (D7), D00K33. http://dx.doi.org/10.1029/2010JD014650.

Fischer, E.V., Perry, K.D., Jaffe, D.A., 2011. Optical and chemical properties of aerosols transported to Mount Bachelor during spring 2010. J. Geophys. Res. 116 (D18), D18202. http://dx.doi.org/10.1029/2011JD015932.

Guasta, M.D., Marini, S., 2000. On the retrieval of urban aerosol mass concentration by a 532 and 1064 nm LIDAR. J. Aerosol Sci. 31 (12), 1469–1488.

Han, Z., Montague, D.C., Snider, J.R., 2003. Airborne measurements of aerosol extinction in the lower and middle troposphere over Wyoming, USA. Atmos. Environ. 37 (6), 789–802.

Hänel, G., 1998. Vertical profiles of the scattering coefficient of dry atmospheric particles over Europe normalized to air at standard temperature and pressure. Atmos. Environ. 32 (10), 1743–1755.

Haywood, J.M., Shine, K.P., 1997. Multi-spectral calculations of the direct radiative forcing of tropospheric sulphate and soot aerosols using a column model. Quart. J. Roy. Meteorol. Soc. A 123 (543), 1907–1930.

He, X., Li, C., Lan, A.K.H., Deng, Z.Z., Mao, J.T., Wang, M.H., et al., 2009. An intensive study of aerosol optical properties in Beijing urban area. Atmos. Chem. Phys. 9 (22), 8903–8915.

Horvath, H., 1995. Estimation of the average visibility in central Europe. Atmos. Environ. 29 (2), 241–246.

Horvath, H., 1996. Spectral extinction coefficients of rural aerosol in southern Italy—a case study of cause and effect of variability of atmospheric aerosol. J. Aerosol Sci. 27 (3), 437–453.

Iqbal, M., 1983. An Introduction to Solar Radiation. Academic Press, Canada, Ont.

Johnson, D.W., Osborne, S., Wood, R., Suhre, K., Quinn, P.K., Bates, T., et al., 2000. Observations of the evolution of the aerosol, cloud and boundary-layer characteristics during the 1st ACE-2 Lagrangian experiment. Tellus B52B (2), 348–374.

Kleefeld, C., O'Dowd, C.D., O'Reilly, S., Jennings, S.G., Aalto, P., Becker, E., et al., 2002. Relative contribution of submicron and supermicron particles to aerosol light scattering in the marine boundary layer. J. Geophys. Res. 107 (D19). http://dx.doi.org/10.1029/2000JD000262 (PAR 8-1–PAR 8-13).

Li, C., Marufu, L.T., Dickerson, R.R., Li, Z., Wen, T., Helas, G., et al., 2007. In situ measurements of trace gases and aerosol optical properties at a rural site in northern China during East Asian Study of Tropospheric Aerosols: an International Regional Experiment 2005. J. Geophys. Res. 112, D22S04. http://dx.doi.org/10.1029/2006JD007592.

Li, Z., Niu, F., Fan, J., Liu, Y., Rosenfeld, D., Ding, Y., 2011. Long-term impacts of aerosols on the vertical development of clouds and precipitation. Nat. Geosci. 4 (12), 888–894.

Li, W.J., Shi, Z.B., Zhang, D.Z., Zhang, X.Y., Li, P.R., Feng, Q.J., et al., 2012. Haze particles over a coal-burning region in the China Loess Plateau in winter: three flight missions in December 2010. J. Geophys. Res. 117 (D12), D12306. http://dx.doi.org/10.1029/2012JD017720.

Li, J., Yin, Y., Li, P., Li, Z., Li, R., Cribb, M., et al., 2015. Aircraft measurements of the vertical distribution and activation property of aerosol particles over the Loess Plateau in China. Atmos. Res. 155, 73–86. http://dx.doi.org/10.1016/j.atmosres.2014.12.004.

Liu, X., Cheng, Y., Zhang, Y., Jung, J.S., Sugimoto, N., Chang, S.Y., et al., 2008. Influences of relative humidity and particle chemical composition on aerosol scattering properties during the 2006 PRD campaign. Atmos. Environ. 42 (7), 1525–1536.

Liu, J., Zheng, Y., Li, Z., Flynn, C., Cribb, M., 2012. Seasonal variations of aerosol optical properties, vertical distribution and associated radiative effects in the Yangtze Delta region of China. J. Geophys. Res. 117 (D16), D00K38. http://dx.doi.org/10.1029/2011jd016490.

Liu, X.G., Li, J., Qu, Y., Han, T.T., Hou, L., Gu, J.W., et al., 2013. Formation and evolution mechanism of regional haze: a case study in the megacity Beijing, China. Atmos. Chem. Phys. 13, 4501–4514.

Petzold, A., Schönlinner, M., 2004. Multi-angle absorption photometry—a new method for the measurement of aerosol light absorption and atmospheric black carbon. J. Aerosol Sci. 35 (4), 421–441.

Petzold, A., Schloesser, H., Sheridan, P.J., Arnott, W.P., Ogrenc, J.A., Virkkulae, A., 2005. Evaluation of multiangle absorption photometry for measuring aerosol light absorption. Aerosol Sci. Technol. 39 (1), 40–51.

Qiu, J., Takeuchi, N., 2001. Effects of aerosol vertical inhomogeneity on the upwelling radiance and satellite remote sensing of surface reflectance. Adv. Atmos. Sci. 18 (4), 539–553.

Raut, J.C., Chazette, P., 2008. Vertical profiles of urban aerosol complex refractive index in the frame of ESQUIF airborne measurements. Atmos. Chem. Phys. 8, 901–919.

Seinfeld, J.H., Pandis, S.N., 1998. Atmospheric Chemistry and Physics: From Air Pollution to Climate Change. John Wiley & Sons, Inc. (1326 pp.).

Sheridan, P.J., Ogren, J.A., 1999. Observations of the vertical and regional variability of aerosol optical properties over central and eastern North America. J. Geophys. Res.: Atmos. (1984–2012) 104 (D14), 16793–16805. http://dx.doi.org/10.1029/1999JD900241.

Snider, J.R., Guibert, S., Brenguier, J.L., 2000. Lack of closure between dry and wet aerosol measurements: results from ACE-2. AIP Conf. Proc. 534 (1), 627–631.

Sun, K., Qu, Y., Wu, Q., Han, T., Gu, J., Zhao, J., et al., 2014. Chemical characteristics of size-resolved aerosols in winter in Beijing. J. Environ. Sci. 26 (8), 1641–1650.

Tao, J., Zhang, L., Cao, J., Hsud, S.C., Xia, X., Zhang, Z., et al., 2014. Characterization and source apportionment of aerosol light extinction in Chengdu, southwest China. Atmos. Environ. 95, 552–562.

Waggoner, A.P., Weiss, R.E., Ahlquist, N.C., Covert, D.S., Will, S., Charlson, R.J., 1981. Optical characteristics of atmospheric aerosols. Atmos. Environ. 15 (10-11), 1891–1909.

Wang, X.M., Chen, J.M., Cheng, T.T., Zhang, R.Y., Wang, X.M., 2014. Particle number concentration, size distribution and chemical composition during haze and photochemical smog episodes in Shanghai. J. Environ. Sci. 26 (9), 1894–1902.

Welton, E.J., Voss, K.J., Quinn, P.K., Flatau, P.J., Markowicz, K., Campbell, J.R., et al., 2002. Measurements of aerosol vertical profiles and optical properties during INDOEX 1999 using micropulselidars. J. Geophys. Res. 107 (D19). http://dx.doi.org/10.1029/2000JD000038 (INX2 18-1–INX2 18-20).

Xu, J., Bergin, M.H., Yu, X., Liu, G., Zhao, J., Carrico, C.M., et al., 2002. Measurement of aerosol chemical, physical and radiative properties in the Yangtze delta region of China. Atmos. Environ. 36 (2), 161–173.

Xu, J., Bergin, M.H., Greenwald, R., Schauer, J.J., Shafer, M.M., Jaffrezo, J.L., et al., 2004. Aerosol chemical, physical, and radiative characteristics near a desert source region of northern China during ACE-Asia. J. Geophys. Res. 109 (D19), D19S03. http://dx.doi.org/10.1029/2003JD004239.

Xu, J.W., Tao, J., Zhang, R.J., Cheng, T.T., Leng, C.P., Chen, J.M., et al., 2012. Measurements of surface aerosol optical properties in winter of Shanghai. Atmos. Res. 109–110, 25–35.

Yan, H., 2007. Aerosol scattering properties in northern China. Atmos. Environ. 41 (32), 6916–6922.

Yan, P., Tang, J., Huang, J., Mao, J.T., Zhou, X.J., Liu, Q., et al., 2008. The measurement of aerosol optical properties at a rural site in Northern China. Atmos. Chem. Phys. 8, 2229–2242.

Yin, Y., Wurzler, S., Levin, Z., Reisin, T.G., 2002. Interactions of mineral dust particles and clouds: effects on precipitation and cloud optical properties. J. Geophys. Res. 107 (D23). http://dx.doi.org/10.1029/2001JD001544 (AAC 19-1–AAC 19-14).

Yin, Y., Chen, C., Chen, K., An, J.L., Wang, W.W., Lin, Z.Y., et al., 2010. An observational study of the microphysical properties of atmospheric aerosol at Mt. Huang. Trans. Atmos. Sci. 33 (2), 129–136.

Zhang, J.H., Mao, J.T., Wang, M.H., 2002. Analysis of the aerosol extinction characteristics in different areas of China. Adv. Atmos. Sci. 19 (1), 136–152.

Zhang, W., Hu, B., Chen, C.H., Du, P., Zhang, L., Feng, G.H., et al., 2004. Scattering properties of atmospheric aerosols over Lanzhou City and applications using an integrating nephelometer. Adv. Atmos. Sci. 21 (6), 848–856.

Zhang, Q., Zhao, C.S., Tie, X.X., Wei, Q., Huang, M.Y., Li, G.H., et al., 2006. Characterizations of aerosols over the Beijing region: a case study of aircraft measurements. Atmos. Environ. 40 (24), 4513–4527.

Zhao, S.P., Yu, Y., Liu, N., He, J.J., Chen, J.B., 2014. Effect of traffic restriction on atmospheric particle concentrations and their size distributions in urban Lanzhou, Northwestern China. J. Environ. Sci. 26 (2), 362–370.